Available online at www.sciencedirect.com
SCIENCE DIRECT®
Journal of Food Engineering 69 (2005) 225–234
JOURNAL OF FOOD ENGINEERING
www.elsevier.com/locate/jfoodeng

Development of multispectral image processing algorithms for identification of wholesome, septicemic, and inflammatory process chickens ☆

Chun-Chieh Yang [a], Kuanglin Chao [b,*], Yud-Ren Chen [b]

[a] University of Kentucky, Lexington, KY 40546-0276, USA
[b] USDA/ARS/ISL, Beltsville, MD 20705-2350, USA

Received 3 November 2003; revised 23 June 2004; accepted 16 July 2004

Abstract

A multispectral imaging system and image processing algorithms for food safety inspection of poultry carcasses were demonstrated. Three key wavelengths of 460, 540, and 700 nm, previously identified using a visible/near-infrared spectrophotometer, were implemented in a common-aperture multispectral imaging system, and images were collected for 174 wholesome, 75 inflammatory process, and 170 septicemic chickens. Principal component analysis was used to develop an algorithm for separating septicemic chickens from wholesome and IP chickens based on average intensity of first component images. A threshold value of 105 was able to correctly separate 95.6% of septicemic chickens. To differentiate inflammatory process chickens, a region of interest was defined from which spectral features were determined. The algorithm was able to correctly identify 100% of inflammatory process chickens by detecting pixels that satisfied the spectral feature conditions. A decision tree model was created to classify the three chicken conditions using inputs from the two image processing algorithms. The results showed that 89.6% of wholesome, 92.3% of inflammatory process, and 94.4% of septicemic chickens were correctly classified.
Published by Elsevier Ltd.

Keywords: Food safety; Machine vision; Poultry

1. Introduction

The Poultry Products Inspection Act (PPIA) requires Food Safety and Inspection Service (FSIS) inspectors of the United States Department of Agriculture (USDA) to conduct post-mortem inspection for wholesomeness of all chickens intended for sale to US consumers (USDA, 1984). Poultry inspection is a complex process. FSIS inspectors are trained to recognize infectious condition and avian diseases, dressing defects, fecal and digestive content contamination, and conditions that are related to many other consumer protection concerns. FSIS has just completed a three-year transformation of its traditional inspection system to a Hazard-Analysis-and-Critical-Control-Point (HACCP) inspection system. Under this new system, FSIS inspectors still do a bird-by-bird organoleptic examination, but FSIS personnel also monitor a producer-run HACCP plan, which is developed by each plant and approved by FSIS. Under HACCP, increasing consumer demand and line speeds will continue to increase the need for and pressure on inspectors. Thus, to address food safety concerns and meet growing consumer demand, there is an urgent need to develop automated inspection systems that can

☆ Mention of trade names or commercial products is solely for the purpose of providing specific information and does not imply endorsement or recommendation by the USDA.

* Corresponding author. Address: USDA/ARS/ISL, Building 303, BARC-East, 10300 Baltimore Avenue, Beltsville, MD 20705-2350, USA. Tel.: +1 301 504 8450; fax: +1 301 504 9466.
E-mail address: chaok@ba.ars.usda.gov (K. Chao).

0260-8774/$ - see front matter Published by Elsevier Ltd.
doi:10.1016/j.jfoodeng.2004.07.021

operate on-line in real-time in the slaughter plant environment. These systems should be able to accurately detect and identify carcasses with infectious condition, particularly septicemia/toxemia. They should also detect avian diseases, particularly airsacculitis, ascites, and inflammatory process (IP).

Machine vision is a non-invasive technology that provides automated production processes with vision capabilities when the majority of inspection tasks are highly repetitive, and their effectiveness depends on the efficiency of the human inspectors. A number of investigators have demonstrated various applications using machine vision techniques for agricultural and food industries, particularly in grading and inspection (Miller & Delwiche, 1989; Precetti & Krutz, 1993; Sakar & Wolfe, 1985; Tao, Morrow, Heinemann, & Sommer, 1990). Although implementations of machine vision technologies have generally concentrated on quality assessments, interest in addressing food safety issues has been steadily increasing in recent years. The broadband spectral characteristics of color machine vision techniques traditionally used in systems for quality assessments have been found less effective for some food safety issues compared to some more recently developed techniques such as multispectral imaging systems (Chen, Chao, & Kim, 2002).

A multiwavelength imaging system could be implemented in several ways: using a filter wheel, a liquid crystal tunable filter (LCTF), several cameras with filters, or a single camera with beamsplitter. A critical issue that should be considered in real-time operations of these devices is the amount of time between sequentially acquired images at different wavelengths. This is a function of both the image capturing speed and band switch speed. Electromechanical filter wheels have limitations in the speed of wavelength switching. Improvement in LCTF technology makes a LCTF system superior to electromechanical filter wheels in both speed and flexibility of spectral selection (Evans, Thai, & Grant, 1997). The time required for the LCTF to switch between wavelengths is approximately 50 ms (Mao & Heitschmidt, 1998). However, this still makes the system unsuitable for synchronization with moving objects during high-speed inspection. Recent advances in optical design make common aperture systems, which allow multispectral (two to four spectral bands) imaging of samples with a single acquisition, promising for real-time operation.

In developing such vision inspection systems it is essential to first identify key wavelengths, then develop algorithms based on those wavelengths, and finally implement them for on-line applications. For example, Windham, Lawrence, Park, and Buhr (2003) and Park, Lawrence, Windham, and Buhr (2002) have used a visible/near-infrared (Vis/NIR) monochromator to identify wavelengths associated with fecal absorption bands, and then, using hyperspectral imaging, evaluated those wavelengths and developed image-processing algorithms. For food safety inspection of poultry carcasses, wavelengths associated with infection conditions have been identified using a visible/near-infrared spectrophotometer (Chao, Chen, & Chan, 2003).

The main objective of this study was to develop multispectral image processing algorithms for the detection of infectious poultry conditions. An imaging system was designed using a multispectral common-aperture camera with three interference filters in the visible wavelength range. Two image-processing algorithms were developed for the specific identification of septicemic and inflammatory process chickens. A decision tree model was constructed for the classification of wholesome, septicemic, and inflammatory process chickens.

2. Materials and methods

2.1. Sample collection

Eviscerated chicken carcasses were identified and collected by USDA FSIS veterinarians from Allen Family Foods (Cordova, MD, USA). A total of 245 unwholesome carcasses (170 septicemia and 75 inflammatory process) and 174 inspected and passed wholesome carcasses were collected over a three-month period in 2003. Septicemia is a systemic disease caused by pathogenic microorganisms in the blood, and its symptoms are visible on the exterior of the carcass. Inflammatory process (IP) is a physiologic condition when the yolk sac was not completely absorbed after hatching and has progressed into a pathological inflammatory process. The IP lesions are normally observed between the skin and the ventral abdominal muscle tissue in the perineal area after the vent is opened and the eviscerator has drawn out the internal visceral organs.

Chicken carcasses were identified according to the condemnation conditions and placed in plastic bags to minimize dehydration. The bags were then placed in coolers, covered with ice, and transported to the Instrumentation and Sensing Laboratory (ISL) located in Beltsville, MD, USA, within 2 h for the experiments.

2.2. Multispectral imaging system

The multispectral imaging system consists of a three-channel common aperture camera (MS2100, Duncan-Tech, Auburn, CA, USA), a frame grabber (PCI-1428, National Instruments, Austin, TX, USA), an industrial computer (BSI, City of Industry, CA, USA), and eight 100-W tungsten halogen lights. The three-channel common aperture camera utilizes a color-separating prism to split broadband light entering the camera through the lens into three optical channels. An interference filter

and charge-coupled-device (CCD) imaging array are placed at each of the three exit planes of the prism. The image acquired by each channel (656 × 493 pixels) is formed by the wavelengths of light that have been passed through each optical path in the prism. Control of the camera settings, such as triggering mode, output bit depth (8 bits), and the integration time of exposure and the analog gain at the CCD sensor before the image was digitized for each imaging channel, is accomplished using the CameraLink utility program (DuncanTech, Auburn, CA, USA). Signals from the CCD imaging arrays are digitized by the frame grabber. From each of the three channels, an 8-bit monochrome image is saved.

2.3. Wavelength selection

The results of a previous study examining visible/near-infrared spectral variations of poultry carcasses (Chao et al., 2003) were considered in selecting the wavelengths for the interference filters. Fig. 1(a) and (b) shows the average reflectance spectra and second difference spectra, respectively, for wholesome and unwholesome chickens. The average reflectance spectra for both wholesome and unwholesome chickens in the region above 650 nm show high percentage reflectance and a lack of distinct spectral features. For this reason, the 700 nm wavelength was selected as one of the three center wavelengths to create masks for image processing. In the second difference spectra, wholesome and unwholesome spectra are significantly different at 460, 490, 540, and 578 nm. From these, 460 and 540 nm were selected for the other two center wavelengths. Consequently, interference filters with center wavelengths at 461.75 nm (full width at half maximum, or FWHM, of 20.78 nm), 541.80 nm (18.31 nm FWHM), and 700.07 nm (17.40 nm FWHM) were used for the three-channel common aperture camera.

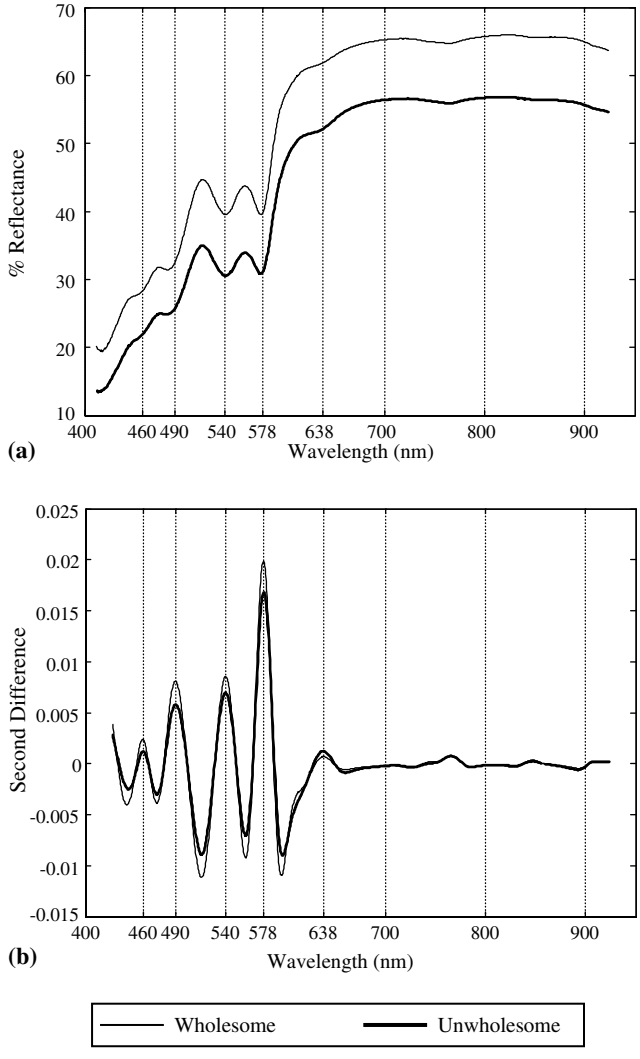

Fig. 1. Percentage reflectance of (a) average spectra and (b) second difference spectra for wholesome and unwholesome chicken images.

2.4. Camera illumination and settings

The layout of the multispectral imaging system is illustrated in Fig. 2. The horizontal distance between the camera lens and the shackle holding the chicken, where located the field of view, is 813 mm. For each channel, the image size is 656 × 493 pixels. The field of view is 397 mm × 298 mm; therefore, the image resolution is 0.37 mm^2 per pixel. Viewed from the shackle position, the eight tungsten halogen lights are arranged in four pairs, with two adjacent pairs 318 mm above the camera and two adjacent pairs 318 mm below the camera. Side by side, the two upper pairs span 190 mm, as do the two lower pairs. Viewed from the side, the upper pairs are positioned 267 mm from the field of view (546 mm from the camera) while the lower pairs are positioned slightly further at 305 mm from the field of view (508 mm from the camera). This lighting arrangement provides more illumination to the lower body of the bird, including the thighs, compensating for what would otherwise be insufficient lighting in the upper image area.

A Spectralon diffuse reflectance target of 99% reflectance (Labsphere, North Sutton, NH, USA) was used as a calibration target to determine the proper integration time and gain for the lighting arrangement described above. It was found that the spectral image was safely below saturation level when the average intensity (across all pixels) was at 200. From this determination, the integration time and gain for the 700 and 540 nm channels were set. The gain and integration time were set at 2 dB and 4.5 ms for 700 nm, and at 3 dB and 5.0 ms for 540 nm. However, using the average pixel intensity of 200 as a guideline, saturation was observed for the 460 nm channel (gain of 9 dB and the integration time of 9.5 ms). To reduce illumination and eliminate saturation for the 460 nm channel, the integration time was

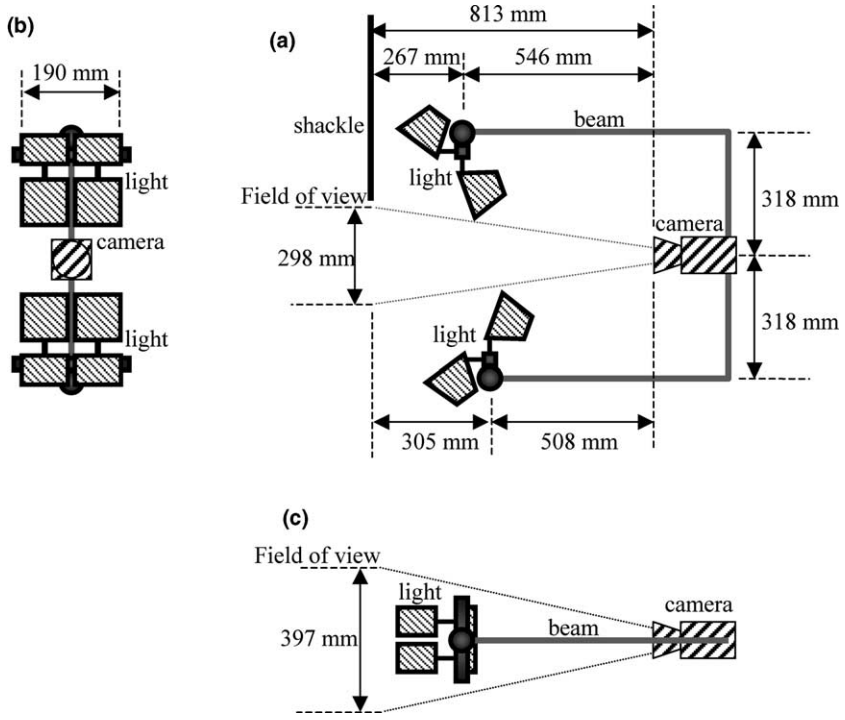

Fig. 2. The layout of a multispectral imaging system for poultry carcass inspection: (a) side view, (b) front view, (c) top view.

reduced to 9 ms while maintaining the gain at 9 dB. These settings were used for relative reflectance calculation and calibration of the chicken images.

Compared to the Spectralon images, the chicken images required longer integration time since the chicken reflectance was much lower than that of the Spectralon. Using the same gain values, integration time was increased until the average image intensity was higher than 120, at which point the image was determined to be clear and without saturation. In this manner, the integration time was then set at 5, 10, and 18 ms for the 700, 540, and 460 nm channels, respectively.

2.5. Multispectral image collection and preprocessing

Images were taken from 174 wholesome chickens, 170 septicemic chickens, and 75 inflammatory process chickens using the CameraLink utility program. Each bird was hung on the shackle with a black background. The front- and back-sides of carcass were imaged. For each chicken three images were simultaneously obtained at 700, 540, and 460 nm. Fig. 3 shows example images for three chickens: one wholesome, one septicemia, and one inflammatory process. It should be noted that on each day some Spectralon images were taken for the relative reflectance calculation on that day in order to eliminate image variation.

Using MATLAB 6.1 (MathWorks, Inc., Natick, MA, USA), three image preprocessing steps were performed, as diagrammed in Fig. 4. First, relative reflectance calculation was performed according to Eq. (1):

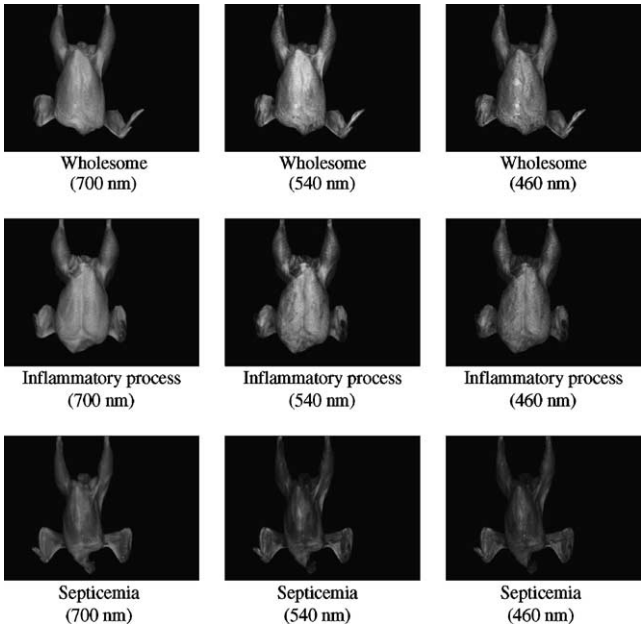

Fig. 3. Example multispectral images of wholesome, septicemic, and inflammatory process chickens at 460, 540, and 700 nm wavelengths.

$$I = \frac{I_0 - B}{W - B}, \tag{1}$$

where I is the relative-reflectance image, I_0 is the original image, B is the dark reference image, and W is the white Spectralon reference image. Second, the 700 nm image was used to build a mask. The intensity for the black background at 700 nm was always below 20, whereas

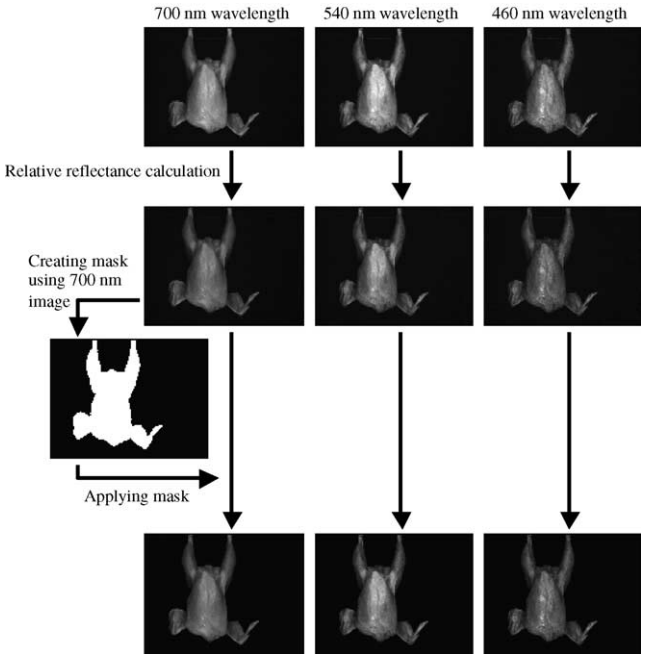

Fig. 4. The diagram of multispectral image collection and preprocessing procedure.

the chicken intensity was always above 20. Thus, the threshold value of 20 was used to create the mask. Third, the mask was applied to each of the three channel images for image segmentation. This resulted in the background pixels of each image being reset to zero; the intensity values for other pixels remained the same.

2.6. Multispectral image processing

Two image processing methods were used in this study: principal component analysis (PCA) and region of interest (ROI) analysis. PCA is a technique used to approximate the original data with lower dimensional feature vectors, since the data from multiple spectral bands often involve a certain degree of redundancy. The basic approach is to compute the eigenvectors of the covariance matrix, and approximate the original data by a linear combination of the leading eigenvectors. For a multispectral image of k spectral channels each with $m \times n$ pixels, the image data is reorganized into two-dimensional array X of size s by k where $s = (m \times n)$. The covariance matrix of X is defined as:

$$C_x = \frac{\overline{X}^{\mathrm{T}}\overline{X}}{s-1}, \tag{2}$$

where C_x is a matrix of size $k \times k$; and $\overline{X}$ is the $s \times k$ mean-centered matrix of X, determined by first calculating the mean for each column, and then subtracting the column mean from each value in that column. In the PCA decomposition, the p_i vectors are eigenvectors of the covariance matrix C_x. For each p_i,

$$C_x p_i = \lambda_i p_i, \tag{3}$$

where λ_i is the eigenvalue associated with the eigenvector p_i. Each principal component PC_i is denoted by

$$PC_i = X_1 p_{1i} + X_2 p_{2i} + X_3 p_{3i} + \cdots + X_k p_{ki}. \tag{4}$$

Each principal component is a weighted sum of the k channel images.

Ten wholesome, 10 inflammatory process, and 10 septicemic chickens were randomly selected from the data collection. For each chicken, the three spectral channel images were mean centered; i.e. for each channel, the average intensity of the image was subtracted from the value of each pixel. Single value decomposition (SVD) was performed using MATLAB to calculate the eigenvectors p_i of the covariance matrix C_x for each of the 30 chickens. The average eigenvector p_i values were calculated for the 30 chickens.

The spectral data for the remaining 164 wholesome, 65 inflammatory process, and 160 septicemic chickens were mean centered, and then the principal components were calculated for each chicken using these mean-centered matrices with the average eigenvector p_i values calculated from the previous 30 chickens. Then, the average intensities of the principal component images were calculated for analysis. This image processing was performed for both front and back images of each chicken.

The ROI analysis was developed for specific area of the chicken carcass. Localized symptoms of inflammatory process occur in the area of the lower abdomen and its junction with the thigh. Therefore, this area was chosen as the ROI for differentiating inflammatory process from other chicken conditions. Generally, the ROI can be observed only from the front-side image. Fig. 5 shows the outline of this ROI. Using edge detection, the central line of the chicken body was determined by the middle point between two drumsticks. Along the

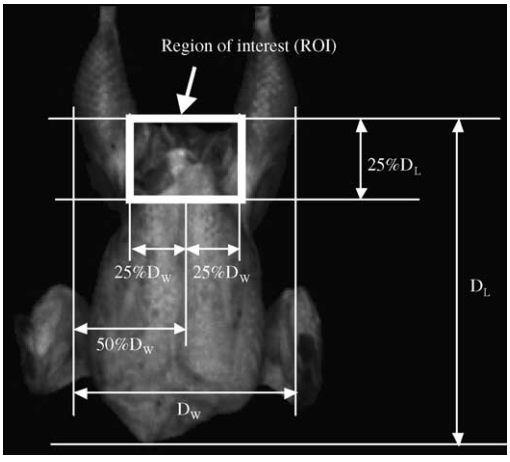

Fig. 5. Definition of the region of interest for differentiating inflammatory process chickens from other chicken conditions.

central line, a 40-pixel (24 mm) wide strip was made up to ensure the proper detection of the chicken body edge. Within the strip, the top and bottom edges of the chicken body were detected and the body length between the two edges, designated as D_L in Fig. 5, was calculated. The top edge was then defined as the top boundary of the ROI. The bottom boundary of the ROI was defined at 25% of body length D_L measured from the top boundary. Within the top and bottom boundaries, the right and left edges of the chicken body were detected. The body width and the center point between the two edges (distance of D_W in Fig. 5) were calculated. From the center point, the right and left boundaries of the region of interest were defined at 25% of D_W to the right and 25% of D_W to the left, respectively.

From each of 10 images of inflammatory process chickens, a 4×4 block of 16 neighboring pixels was selected from an area showing inflammatory process symptoms within the ROI, for a total of 160 pixels. Another 160 sample pixels were selected within the ROI from 10 wholesome chicken images, and another 160 from 10 septicemic chicken images. The intensities of these 480 sample pixels at each of the three wavelengths were analyzed to generate representative features or equations to differentiate inflammatory process chickens from other chicken conditions. The generated features would be presented in Section 3.

2.7. Image classification

A decision tree model uses a machine-learning algorithm that learns the input/output pattern from training data and generates a series of if-then decision rules to appropriately represent the pattern (Breiman, Friedman, Olshen, & Stone, 1984; Han & Kamber, 2001; Yang et al., 2003). The structure of a decision tree model can be represented by a flowchart diagram such as that shown in Fig. 6. At the top of the decision tree, a "root node" represents the entire data set. According to an if-then decision rule, the data set is divided into two groups, represented by two "child nodes". This completes one new tree level. Like the root node, each child node in this first level becomes a "mother node" for the next level, i.e. each set is divided again using an if-then decision rule to create two groups represented by two new child nodes. These subsequent child nodes either also become mother nodes, or become "terminal nodes". At a terminal node, further divisions are prevented if (1) all the data belong to the same output category, or (2) the conditions of a stopping rule are met.

The C&RT algorithm (AnswerTree 3.0, SPSS, Chicago, IL, USA) was used in this study to create a decision tree model for classification of chicken conditions. The computer program AnswerTree would automatically generate the decision tree model that contained several decision rules. The details of model generating could be referred to Breiman et al. (1984) and Yang et al. (2003). For each chicken, there were two input variables for the model: the principal component image intensities and pixels in the region of interest as identified by representative features for inflammatory process. The output variable was the chicken category: wholesome, septicemia, or inflammatory process. To determine the proper stopping rules, a sensitivity analysis was carried out using 25 wholesome, 25 inflammatory process, and 25 septicemic chickens randomly selected from the data. The result found that the classification accuracy was reduced when the data set contain more than five chickens at a mother node, or more than two chickens at a terminal node. Also, the performance of decision tree could not be improved further when the decision tree level was more than six. Therefore, three stopping rules were used to avoid over-fitting: (1) At a mother node, the data set must contain at least five chickens; (2) a terminal node must contain at least two chickens; and (3) the maximum number of tree levels is six. Ten-fold cross-validation was used for creating this classification model. The data, consisting of 164 wholesome, 65 inflammatory process, and 160 septicemic chickens, were first randomly split into 10 subgroups. A decision tree was generated with nine of the 10 subgroups and validated by the remaining subgroup. This process was repeated ten times, using each subgroup once for validation, and the overall successful classification rate was determined.

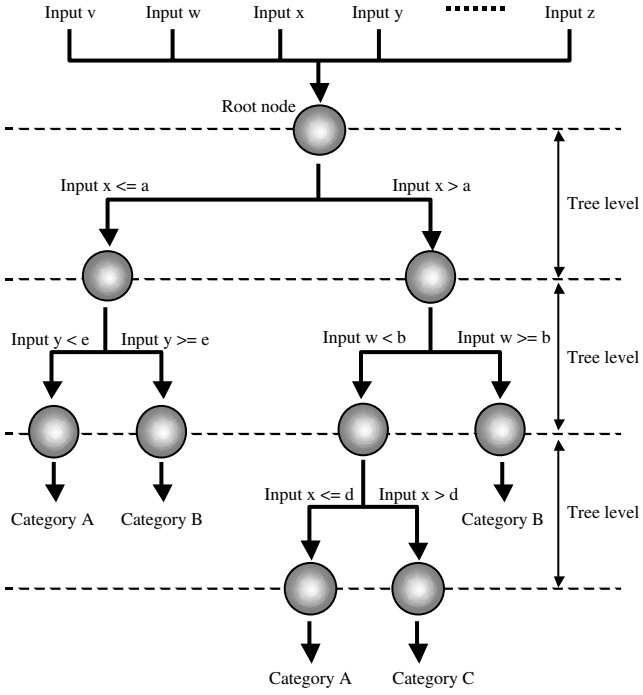

Fig. 6. The general flowchart-like, top-down structure of a decision tree.

3. Results and discussion

3.1. Image processing—principal component analysis

Using PCA for 10 wholesome, 10 inflammatory process, and 10 septicemic sample chickens, the covariance eigenvectors and eigenvalues for each spectral channel were calculated. For the front-side chicken images, the first principal component (PC_1) was found to account for 97.6–99.5% of the total variance. For the back-side chicken images, PC_1 accounted for 98.1–99.4% of the total variance. These results showed that the first principal component images could adequately represent the total variance of the original images. Table 1 shows the average and standard deviation for the PC_1 covariance eigenvector for front- and back-side images of the 30 chickens.

The covariance eigenvectors were used to determine the value of PC_1 for each pixel in an image according to the equations below:

$$\text{(front-side)}\quad PC_1 = \overline{X}_{700} \times 0.6567 + \overline{X}_{540} \times 0.5882 + \overline{X}_{460} \times 0.4556, \tag{5}$$

$$\text{(back-side)}\quad PC_1 = \overline{X}_{700} \times 0.6587 + \overline{X}_{540} \times 0.5794 + \overline{X}_{460} \times 0.4739, \tag{6}$$

where $\overline{X}_{700}, \overline{X}_{540}, \overline{X}_{460}$ are the mean-centered reflectance images at the 700, 540, and 460 nm spectral channels, respectively. PC_1 was calculated for 164 wholesome, 65 inflammatory process, and 160 septicemic chickens using these equations.

For each chicken, the average intensities of the PC_1 front-side image and back-side image were calculated. Fig. 7 shows correlation plots for the front- and back-side images in each category. The linear regression correlation coefficients were relatively high: 0.63 for wholesome, 0.78 for inflammatory process, and 0.69 for septicemic chickens.

Fig. 8 shows a plot of the front- and back-side average PC_1 pixel intensities for all three categories, with the intensity threshold of 105 marked. For front-side chicken images, 95.6% (153 out of 160) of septicemic chickens fell below this threshold while 70.8% (46 out of 65) of inflammatory process chickens and 90.9% (149 out of 164) of wholesome chickens were above that threshold. For back-side chicken images, 87.2% (140 out of 160) septicemic chickens fell below this threshold while 80.0% (52 out of 65) of inflammatory process chickens and 87.2% (143 out of 164) were above that threshold.

The average PC_1 intensity for septicemic chickens appears to be significantly lower than that of wholesome and inflammatory process chickens. Using the threshold

Table 1
The average covariance eigenvectors and standard deviations of the first principal component for three wavelengths and for front- and back-side of chicken images

		Wavelength		
		700 nm	540 nm	460 nm
Front-side	Eigenvector	0.6567	0.5882	0.4556
	Standard deviation	0.0503	0.0535	0.1011
Back-side	Eigenvector	0.6587	0.5793	0.4739
	Standard deviation	0.0498	0.0383	0.0448

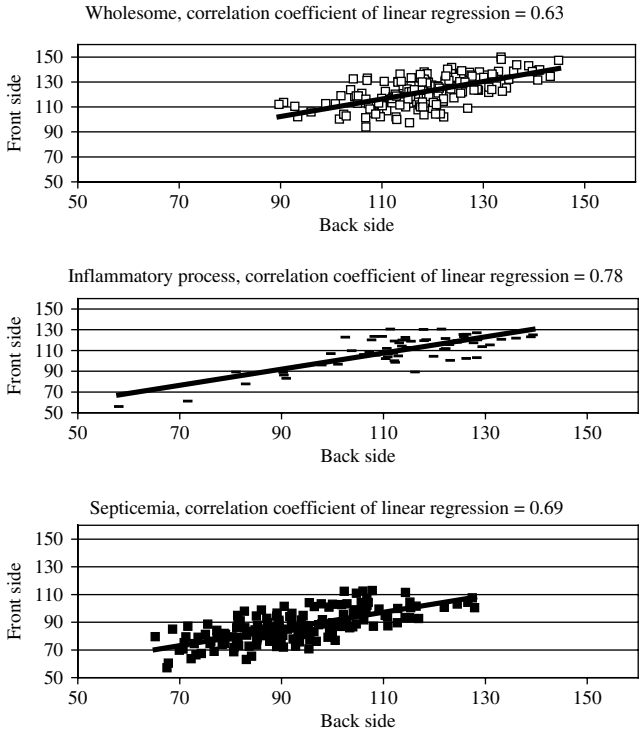

Fig. 7. Linear correlation plots for the front- and back-side of chicken images.

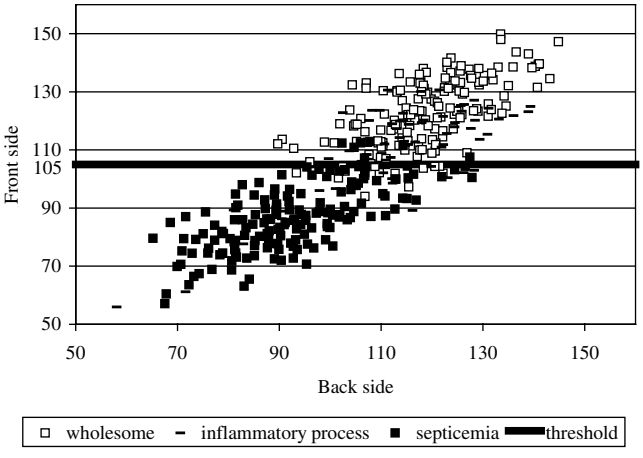

Fig. 8. The average first-principal-component intensities of chicken images and the threshold intensity to differentiate septicemic chickens from other chicken conditions.

of 105, wholesome and inflammatory process chickens are not clearly distinguished from each other. However, the front-side images appear to result in better separation for septicemic chickens than the back-side images do.

3.2. Image processing—region of interest analysis

Table 2 shows statistics for the 480 sample pixels from the ROI areas from 10 chicken images for each category. Compared to the wholesome and septicemia conditions, the intensity of the inflammatory process condition appears to be higher at 540 nm and lower at 460 nm.

Based on the trail-and-error sensitivity analysis, it was found that the ratio of intensity of two wavelengths could be used to separate more inflammatory process chickens from others. Three ratio combinations were tested by sensitivity analysis and the criteria were selected when the highest classification accuracy was obtained. Thus, three representative features were generated to differentiate pixels showing inflammatory process chicken condition from wholesome and septicemia pixels. In the following rules, based on the spectral intensities of the ROI pixels which could be influenced by the presence of deoxymyoglobin and oxymyoglobin, I_{700} is the intensity at 700 nm, I_{540} is the intensity at 540 nm, and I_{460} is the intensity at 460 nm:

$$\frac{I_{540}}{I_{460}} > 2.18, \tag{7}$$

$$\frac{I_{540}}{I_{700}} > 0.85, \tag{8}$$

$$\frac{I_{460}}{I_{700}} < 0.68. \tag{9}$$

After these features were determined, all pixels in the ROI for all of the chicken images were analyzed. Pixels that satisfied all three-feature conditions were identified as inflammatory process pixels, and chicken images containing those pixels were classified as inflammatory process chickens.

As shown in Fig. 9, 100% of inflammatory process chickens (65 chickens) contained pixels satisfying all three features (Eqs. (7)–(9)) within the ROI and thus were correctly identified as inflammatory process chickens. Also from Fig. 9, 88.4% of wholesome chickens (145 out of 164 chickens) and 80.6% of septicemic chickens (129 out of 160 chickens) contained no pixels identified by all three feature rules and thus were correctly identified as non-inflammatory process chickens. The erroneous classification of 11.6% of wholesome and 19.4% of septicemic birds as inflammatory process birds due to 50 or fewer pixels, was considered acceptable since the feature rules were designed to err on the side of misidentification of wholesome and septicemic birds rather than to misidentify inflammatory process birds. Approximately 24.6% (16 of 65) inflammatory process birds were correctly classified by ROI analysis due to 10 or fewer pixels out of the total ROI area. Since the area in which an eviscerated bird will show signs of the inflammatory process condition is limited to the exposed meat around the vent opening, an effective analysis method needs to be capable of detecting very small areas such as the ten-pixel area of 3.70 mm^2.

3.3. Image classification—combination of image processing analyses

Because the results found that either PCA or ROI method could separate only one unwholesome chicken condition from others, it is necessary to combine two methods as one process. To apply two methods sequentially, one method was applied first on all chickens in order to separate condemned chickens, and another method was applied to chickens not condemned by the first method. Table 3 shows the results of applying the PCA and ROI methods sequentially. Applying the PCA method to all chickens followed by applying the ROI analysis to uncondemned chickens by the PCA method, 79.9% of wholesome (131 out of 164), 70.8% of inflammatory process (46 out of 65), and 95.6% of septicemic chickens (153 of out 160) could be correctly identified. When applying the ROI method first to all

Table 2
Statistics for intensities of 160 sample pixels within the region of interest region of interest for each chicken condition

		Minimum	Maximum	Average	Standard deviation
Wholesome	700 nm	71	112	88.9	9.1
	540 nm	55	117	77.9	13.9
	460 nm	40	91	59.3	11.9
Inflammatory process	700 nm	67	131	100.8	15.5
	540 nm	56	135	93.1	17.5
	460 nm	19	75	47.0	13.5
Septicemia	700 nm	64	119	90.7	16.6
	540 nm	35	128	63.9	26.5
	460 nm	25	101	49.2	19.7

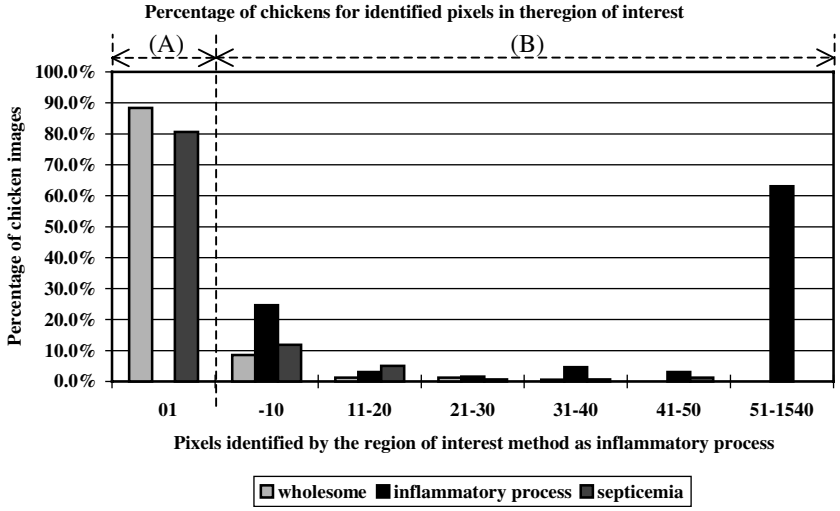

Fig. 9. The percentage of chicken images identified by the spectral features within the region of interest for each category of chickens based on the numbers of pixels that satisfied the conditions of Eqs. (7)–(9): group (A) classified as non-inflammatory process, and group (B) classified as inflammatory process.

Table 3
Classification accuracy and misclassification matrix for the amounts and the percentages of chickens classified by combination of principal component analysis (PCA) and region of interest analysis (ROI)

Sequence of application	Classification	Real conditions		
		Wholesome	Inflammatory process	Septicemia
PCA, then ROI	Wholesome	**131** **(79.9%)**	0 (0%)	7 (4.4%)
	Inflammatory process	18 (11.0%)	**46** **(70.8%)**	0 (0%)
	Septicemia	15 (9.1%)	19 (29.2%)	**153** **(95.6%)**
ROI, then PCA	Wholesome	**131** **(79.9%)**	0 (0%)	7 (4.4%)
	Inflammatory process	19 (11.6%)	**65** **(100%)**	30 (19.4%)
	Septicemia	14 (8.5%)	0 (0%)	**122** **(76.3%)**

chickens and the PCA method afterwards to un-condemned chickens by the ROI method, the same classification accuracy for wholesome chickens was obtained; 100% of inflammatory process (65 out of 65) and 76.3% of septicemic chickens (122 out of 160) were correctly classified. In both cases, no inflammatory process birds and only 7 of 160 septicemic birds were misclassified as wholesome. However, 20% of wholesome birds were misclassified into one of the unwholesome categories, and a high classification rate could only be obtained for only one unwholesome condition or the other: either septicemia or inflammatory process, but not both.

3.4. Image classification—decision tree model

The decision tree model developed in this study used 15 decision rules based on outputs from the two image processing algorithms. The decision rules included 10 threshold PCA image intensities and five threshold ROI pixel counts. For the root node, the model selected threshold value 104.3 PCA image intensity as the decision rule for the first data division. This threshold was very close to the 105 threshold that was used in the PCA image processing method. Table 4 shows the results for the decision tree model. The model correctly classified 89.6% of wholesome (147 out of 164), 92.3% of inflammatory process (60 out of 65), and 94.4% of septicemic chickens (151 out of 160). Compared to the results from using the two image processing algorithms sequentially (in Table 3), the decision tree performed better in classifying the chickens into multiple individual categories. The decision tree model improved the classification rate of wholesome chickens by 10.4%, and resulted in high classification rates for unwholesome

Table 4
Classification accuracy and misclassification matrix for the amounts and the percentages of chickens classified by the decision tree model

	Classification	Real conditions		
		Wholesome	Inflammatory process	Septicemia
Decision tree	Wholesome	**147 (89.6%)**	2 (3.1%)	8 (5.0%)
	Inflammatory process	5 (3.1%)	**60 (92.3%)**	1 (0.6%)
	Septicemia	12 (7.3%)	3 (4.6%)	**151 (94.4%)**

categories, 94.4% for septicemia and 92.3% for inflammatory process. The PCA and ROI image processing algorithms were developed for targeted classification of single unwholesome categories but were unable to handle multiple categories well. Even though two methods could be used sequentially, the significant variation of image intensity from different chicken conditions may require more than single threshold from each method for proper classification. On the contrary, through the decision tree model using 15 thresholds of decision rules, the capabilities of both methods were combined to simultaneously handle both unwholesome categories as well as the wholesome category.

4. Conclusions

Multispectral images of wholesome, septicemic, and inflammatory process chickens were collected using a common-aperture camera with the interference filters at 460, 540, and 700 nm. After principal component analysis was applied to the multispectral images, separation of septicemic chickens was performed by calculating the average intensity of the first principal component images. The average intensity value for 95% of the septicemic chickens was below the threshold value of 105 and thus those chickens could be correctly differentiated from wholesome and inflammatory process chickens. For separating inflammatory process chickens from wholesome and septicemic chickens, a region of interest was defined around the lower abdomen in the multispectral chicken images and spectral features for inflammatory process were determined. All inflammatory process chickens were successfully separated by the algorithm's identification of pixels satisfying those spectral feature conditions. While these two algorithms were each effective at separating a single category of unwholesome chickens from the wholesome and other unwholesome categories, neither one alone was effective in classifying multiple categories. A decision tree model was constructed to classify chickens based on input from both algorithms, and was able to correctly classify 89.6% of wholesome, 94.4% of septicemic, and 92.3% of inflammatory process chickens.

References

Breiman, L., Friedman, J. H., Olshen, R. A., & Stone, C. J. (1984). *Classification and regression trees*. Belmont, CA, USA: Wadsworth.

Chao, K., Chen, Y. R., & Chan, D. E. (2003). Analysis of Vis/NIR spectral variations of wholesome, septicemia, and cadaver chicken carcasses. *Applied Engineering in Agriculture, 19*(4), 453–458.

Chen, Y. R., Chao, K., & Kim, M. S. (2002). Future trends of machine vision technology for agricultural applications. *Computers and Electronics in Agriculture, 36*(2–3), 173–191.

Evans, M. D., Thai, C. N., & Grant, J. C. (1997). Computer control and calibration of a liquid crystal tunable filter for crop stress imaging. *1997 ASAE Annual Meeting, Paper no. 973141*. St Joseph, MI, USA: American Society of Agricultural Engineers.

Han, J., & Kamber, M. (2001). *Data mining: concepts and techniques*. San Diego, CA, USA: Academic Press.

Mao, C., & Heitschmidt, J. (1998). Hyperspectral imaging with liquid crystal tunable filter for biological and agricultural assessment. *Proceedings of SPIE* (3543, pp. 172–181). Bellingham, WA, USA: The International Society for Optical Engineering.

Miller, B. K., & Delwiche, M. J. (1989). A color vision system for peach grading. *Transactions of the ASAE, 34*(4), 1484–1490.

Park, B., Lawrence, K. C., Windham, W. R., & Buhr, R. J. (2002). Hyperspectral imaging for detecting fecal and ingesta contamination on poultry carcasses. *Transactions of the ASAE, 45*(6), 2017–2026.

Precetti, C. J., & Krutz, G. W. (1993). Real-time color classification system. *1993 ASAE Annual Meeting, Paper no. 933002*. St Joseph, MI, USA: American Society of Agricultural Engineers.

Sakar, N., & Wolfe, R. R. (1985). Feature extraction techniques for sorting tomatoes by computer vision. *Transactions of the ASAE, 28*(3), 970–979.

Tao, Y., Morrow, C. T., Heinemann, P. H., & Sommer, J. H. (1990). Automated machine vision inspection of potatoes. *1990 ASAE Annual Meeting, Paper no. 903531*. St Joseph, MI, USA: American Society of Agricultural Engineers.

USDA. (1984). *A review of the slaughter regulations under the Poultry Products Inspection Act*. Washington, D.C., USA: Regulations Office, Policy and Program Planning, FSIS, USDA.

Windham, W. R., Lawrence, K. C., Park, B., & Buhr, R. J. (2003). Visible/NIR spectroscopy for characterizing fecal contamination of chicken carcasses. *Transactions of the ASAE, 46*(3), 747–751.

Yang, C.-C., Prasher, S. O., Enright, P., Madramootoo, C., Burgess, M., Goel, P. K., et al. (2003). Application of decision tree technology for image classification using remote sensing data. *Agricultural Systems, 76*(3), 1101–1117.